sciendo

*Int. J. of Applied Mechanics and Engineering, 2022, vol.27, No.1, pp.78-90*
DOI: 10.2478/ijame-2022-0006

# TRANSIENT FLOW THROUGH A POROUS CHANNEL WITH RAMPED PRESSURE GRADIENT AND VELOCITY SLIP BOUNDARY CONDITION

Basant K. JHA and Zainab Sa'id YUNUS*
Department of Mathematics, Ahmadu Bello University, Zaria, NIGERIA
E-mail: zainabsaidyunus95@gmail.com

A transient flow formation of an incompressible fluid through a horizontal porous channel assuming a ramped pressure gradient is considered with the velocity slip boundary conditions. The flow is a laminar flow caused by ramped pressure gradient along the flow direction. The equation governing the flow is modeled, and solved by the Laplace transformation technique to obtain a semi-analytical solution under slip boundary conditions. It was noted that the flow velocity increases as the slip parameter is increased.

**Keywords:** transient flow, velocity slip, ramped pressure gradient, Riemann-Sum approximation technique**.**

## 1. Introduction

Fluid flow in a porous channel is a known problem that occurs in many physical situations such as in filtration processes, material processing, and in water bodies [1]. Fang [2, 3] studied the fluid flow through a horizontal porous channel that allows mass suction and injection, where the influence of mass transfer on the transitory velocity distribution and temperature profiles were analysed. The problem of a fully developed laminar flow of a viscous incompressible fluid through a horizontal porous channel with bottom injection and top suction was studied in the presence of a constant pressure gradient [4]. It was found that the average velocity decreases with increasing the Reynolds number. Khaled and Vafai [5] analyzed the Stokes and Couette flows created by an oscillatory motion at the wall, when the slip boundary condition is assumed. It was noticed that the wall slip decreases the transitory velocity for the Stokes flow while a little transitory effect was noticed for the Couette flow for larger and smaller values of the wall slip coefficient and gap thickness, respectively. A study on the unsteady hydromagnetic Couette flow through a porous channel, caused by the ramped motion of one of the porous plates was carried out. It was assumed that the horizontal channel was formed by two porous plates of uniform permeability, where suction and injection occur at the same rate [6]. Authors in [7] analyzed the transitory free convection and mass transfer flow of an incompressible fluid through a vertical channel when the Dufour effect is present. The plates bounding the channel are assumed to have species concentration as well as ramped wall temperature. The study reveals that the ramped boundary conditions make the flow variables lower compared to the case of constant boundary conditions.

The slip boundary condition or partial slip boundary conditions are often encountered in several types of fluid flow configuration, especially in ducts, tubes and annulus, and they are mostly considered for obtaining accurate results. Jha and Gambo [8] studied the hydrodynamic behavior of slip flow in a curvilinear concentric cylinder, assuming an exponentially growing time-dependent pressure gradient. It was noticed that high level of Dean velocity is achieved due to the exponentially growing time-dependent pressure gradient as well as the slip wall coefficient. Ahmad *et al.* [9] studied the MHD fluid flow of an incompressible viscous fluid near an infinite plate in a rotating frame, accelerating periodically with slippage condition. It was noted that higher values of the slip parameter which represents lower roughness at the surface, reduce both the axial and transverse velocities. Nagayama *et al.* [10] carried out an experimental

* To whom correspondence should be addressed

study on the effects of the boundary condition at the solid-liquid interface on the single-phase convective heat transfer characteristics in microchannel or nanochannel flow. They observed that the solid-liquid interfacial resistance which can be expressed as the slip length or thermal slip length can be ignored when these lengths are comparable with the hydraulic diameter. Wang [11] studied the interaction between surface slip and system rotation orthogonal to the flow direction. It was found that for Poiseuille flow, slip increases the longitudinal flow rate at low rotation and decreases it at high rotation. Fang and Lee [12] solved exactly the transitory incompressible Couette flow and fully developed temperature profiles for slightly rarefied gases, through a channel with porous walls. It was noticed that the slip parameter can alter the heat transfer characteristics and temperature profiles at the walls. Wang [13] discussed briefly the review of analytical solutions for slip- flow in channels and ducts. These analytical findings are used as accuracy standards for estimate methods involving numerical and semi-numerical approach. An investigation on an unsteady Dean flow of an incompressible fluid with homogenous slip, non-homogenous slip, and no-slip boundary condition was conducted [14]. It was noticed that the velocity profile of the fluid amplifies at the wall with the greatest slip coefficient. Jha and Aina [15] considered the thermal as well as hydrodynamic steady flow through a vertical micro-porous-channel(MPC) subjected to suction and injection along the porous plates and assuming a temperature jump and velocity slip at the boundaries. It was noticed that the possibility of transpose flow formation reduces at the cold wall of the channel as the Knudsen number of the velocity slip parameter grows. The laminar pressure driven flow through a horizontal porous channel with velocity slip, was studied in [16]. The computer extended series (CES) and homotopy analysis methods (HAM) were adopted to solve the flow equation due to the advantages they offer. The influence of non-zero velocity slip and pressure gradient were analysed.

This article studies the influence of velocity slip on the transient flow of an incompressible viscous fluid through a horizontal porous channel with top suction and bottom injection presented by [2], where we assume a ramped pressure gradient as well as velocity slip boundary condition. The novelty of this work is the investigation of the effect of the ramped pressure gradient and velocity slip boundary conditions on velocity profile of transient flow formation in a horizontal porous channel with suction/injection. The mathematical formulation is presented in section 2 of the paper, where the dimensionless equations governing the flow were solved subject to the boundary conditions of [2]. The equations were transformed to the Laplace domain by using the Laplace transformation technique, Riemann-Sum approximation technique was applied to transform the equations back to time domain. Numerical values extracted from the equations in the time domain were used for the plotting of graphs.The physical properties of the graphs were also discussed.

## 2. Mathematical formulation

We examine the transitory flow of an incompressible fluid with slip velocity boundaries, in a horizontal porous channel in the presence of a ramped pressure gradient along the flow direction within the porous channel where the lower plate is subjected to mass injection velocity $v_w$ and the upper plate is subjected to mass suction velocity $v_w$.

The $x$-axis is selected along the lower porous plate and the $y$-axis is orthogonal to it. Initially, at $t \le 0$, the plates and the fluid are assumed to be at rest. At $t > 0$ the fluid starts to move due to the application of a ramped pressure gradient $\frac{dp}{dx} = P_0 F(t)$ along the plate direction. The flow is described by the following equations.

$$\rho \frac{\partial u}{\partial t} + \rho v_w \frac{\partial u}{\partial y} = -\frac{dp}{dx} + \mu \frac{\partial^2 u}{\partial y^2} \tag{2.1}$$

with initial and boundary conditions as:

$$t \le 0: \; u = 0 \qquad \text{for} \qquad 0 \le y \le h, \tag{2.2}$$

$$t>0:\begin{cases} u=\beta_1'\left.\dfrac{du}{dy}\right|_{y=0} & \text{at} \quad y=0, \\ \\ u=-\beta_2'\left.\dfrac{du}{dy}\right|_{y=h} & \text{at} \quad y=h. \end{cases} \tag{2.3}$$

The dimensionless form of equation (2.1) can be obtained as follows by defining the following

$$U=\frac{u}{U_0}, \qquad Y=\frac{y}{h}, \qquad \text{and} \qquad T=\frac{tv}{h^2},$$

as used in Fang [2]. Also, $U_0=\dfrac{h^2}{\mu}(-P_0)$, with $\beta_1=\dfrac{\beta_1'}{h}$ and $\beta_2=\dfrac{\beta_2'}{h}$, where $\beta_1'$ and $\beta_2'$ are the slip coefficients in dimensional form.

Therefore equation (2.1) becomes:

$$\frac{\partial U}{\partial T}+\mathrm{Re}\frac{\partial U}{\partial Y}=F(T)+\frac{\partial^2 U}{\partial Y^2}, \tag{2.4}$$

where

$$\mathrm{Re}=\frac{v_w\, h}{v}$$

is the Reynold number that is the mass transfer parameter.

Subjected to the following boundary conditions.

$$T\le 0:\ U=0 \ \ at\ 0\le Y\le 1, \tag{2.5}$$

$$T>0:\begin{cases} U=\beta_1\left.\dfrac{dU}{dY}\right|_{Y=0} & at\, Y=0, \\ \\ U=-\beta_2\left.\dfrac{dU}{dY}\right|_{Y=1} & at\, Y=1 \end{cases} \tag{2.6}$$

where $F(T)$ is defined as follows,

$$F(T)=\frac{1}{T_0}\left[TH(T)-(T-T_0)H(T-T_0)\right]. \tag{2.7}$$

$H(T)$ is the Heaviside unit step function as defined in Jha and Jibril [6],

$$H(T)=\begin{cases} 0, & T<0, \\ \\ 1, & T\ge 0. \end{cases} \tag{2.8}$$

### 2.1. Problem solution

#### 2.1.1. Transient solution

We apply the Laplace transformation technique to equations (2.4)-(2.6) such that $L\left[U\left(Y,T\right)\right]=\bar{U}\left(Y,s\right)=\int_0^\infty U\left(Y,T\right)e^{-sT}dT,$ as defined in Jha and Jibril [6] then,

$$\frac{d^2\bar{U}}{dY^2}-Re\frac{d\bar{U}}{dY}-s\bar{U}=-\bar{F}\left(s\right), \tag{2.9}$$

$$T>0:\begin{cases}\bar{U}=\beta_1\left.\dfrac{d\bar{U}}{dY}\right|_{Y=0} & \text{at} \quad Y=0,\\ \bar{U}=-\beta_2\left.\dfrac{d\bar{U}}{dY}\right|_{Y=1} & \text{at} \quad Y=1,\end{cases} \tag{2.10}$$

$$L\left(F\left(T\right)\right)=\bar{F}\left(s\right)=\frac{\left[1-\exp\left(-sT_0\right)\right]}{s^2T_0} \tag{2.11}$$

where $s$ is the Laplace parameter.

The solution to equation (2.9) under boundary conditions (2.10), is obtained by the method of undetermined coefficients as:

$$\bar{U}\left(Y,s\right)=\exp\left(\frac{\mathrm{Re}}{2}y\right)\left[C_1\cosh\left(\delta y\right)+C_2\sinh\left(\delta y\right)\right]+\frac{\bar{F}\left(s\right)}{s} \tag{2.12}$$

where $\delta=\sqrt{\frac{\mathrm{Re}^2}{4}+s}$. (2.13)

The constants $C_1$ and $C_2$ are defined in the Appendix.

The solutions to equations (2.9) and (2.10) in the time domain are obtained through the application of the Riemann-Sum approximation technique which is a tool used for transforming equations from the Laplace domain into the time domain [8].

The velocity equation can be expressed in the time domain as:

$$L^{-1}\left(\bar{U}\left(Y,s\right)\right)=U\left(Y,T\right)=\frac{e^{\varepsilon T}}{T}\left[\frac{1}{2}\bar{U}\left(Y,s\right)+\mathrm{Re}^{*}\sum_{n=1}^{z}\bar{U}\left(Y,\varepsilon+\frac{i\pi T}{T}\right)\left(-1\right)^n\right] \tag{2.14}$$

where $\mathrm{Re}^{*}$ represents the real part of the summation, $i=\sqrt{-1}$ is the imaginary number, $z$ is the number of terms included in summing up, and $\varepsilon$ is the real part of the Bromwich contour used in the inversion of Laplace transform, following [8].

The skin friction for the lower and upper plates is evaluated as:

$$\left.\frac{d\bar{U}}{dY}\right|_{Y=0}=\left(\frac{\mathrm{Re}}{2}\right)C_1+\delta C_2, \tag{2.15}$$

$$\left.\frac{d\bar{U}}{dY}\right|_{Y=1} = \left(\frac{\mathrm{Re}}{2}\right)\exp\left(\frac{\mathrm{Re}}{2}\right)\left[C_1\cosh(\delta)+C_2\sinh(\delta)\right]+$$
$$+\exp\left(\frac{\mathrm{Re}}{2}\right)\delta\left[C_1\sinh(\delta)+C_2\cosh(\delta)\right]. \tag{2.16}$$

### 2.1.2. Steady state solution

The flow velocity represented by the velocity equation will be constant as the flow time increases, at that time the steady state is attained. Therefore the steady state velocity equation is obtained as

$$\frac{d^2U_s}{dY^2}-\mathrm{Re}\frac{dU_s}{dY}=-1, \tag{2.17}$$

$$U=\beta_1\left.\frac{dU_s}{dY}\right|_{Y=0} \quad \text{at} \quad y=0,$$
$$U=-\beta_2\left.\frac{dU_s}{dY}\right|_{Y=1} \quad \text{at} \quad Y=1. \tag{2.18}$$

The steady state solution is obtained from Eq.(2.17) and boundary conditions (2.18) as

$$U_s(Y)=\frac{Y}{\mathrm{Re}}+\frac{1}{\mathrm{Re}^2}-\frac{D_1}{\mathrm{Re}}+D_2 exp(\mathrm{Re}Y). \tag{2.19}$$

where $D_1$ and $D_2$ are constants defined in the appendix.

The steady-state skin frictions are obtained as:

$$\left.\frac{dU_s}{dY}\right|_{Y=0}=\frac{1}{\mathrm{Re}}+D_2\mathrm{Re}, \tag{2.20}$$

$$\left.\frac{dU_s}{dY}\right|_{Y=1}=\frac{1}{\mathrm{Re}}+D_2\,\mathrm{Re}\,exp(\mathrm{Re}). \tag{2.21}$$

## 3. Results and discussion

The developed and transitory velocity equations were solved in the previous part for fluid flow through a horizontal porous channel with a ramped pressure gradient. In this part of the article, the physical properties of the equations that were obtained in the previous part of the article were discussed. Two cases of velocity slip are presented, we have the homogenous slip and non-homogenous slip boundary conditions.

**CASE I**: Homogenous slip.

We present the velocity profiles of the flow of an incompressible viscous fluid assuming a ramped pressure gradient as well as homogenous slip coefficients represented by the situation when $\beta_1=\beta_2=\beta$.

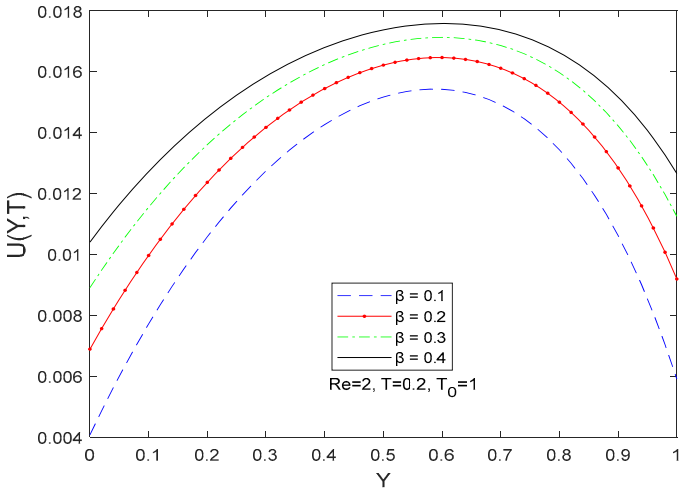


Fig.1 Velocity profile for different values of β, corresponding to the ramped pressure gradient.

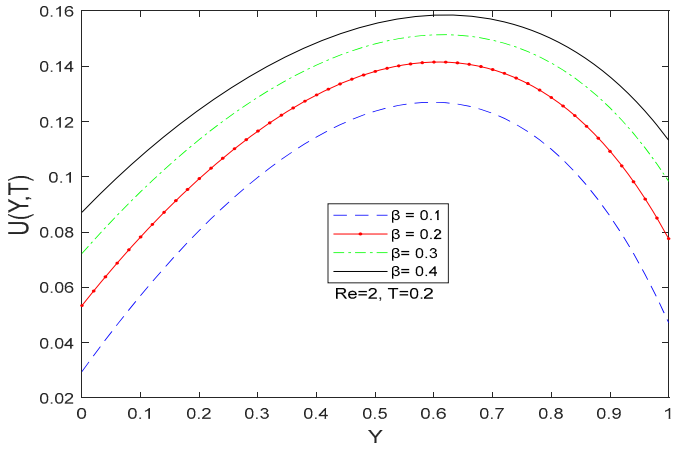


Fig.2. Velocity profile for different values of β, corresponding to the constant pressure gradient.

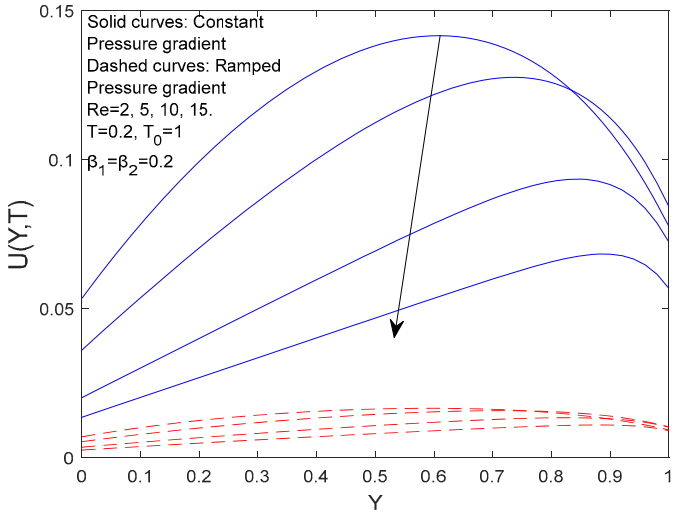


Fig.3. Velocity profile for different values of Re, corresponding to constant and ramped pressure gradient.

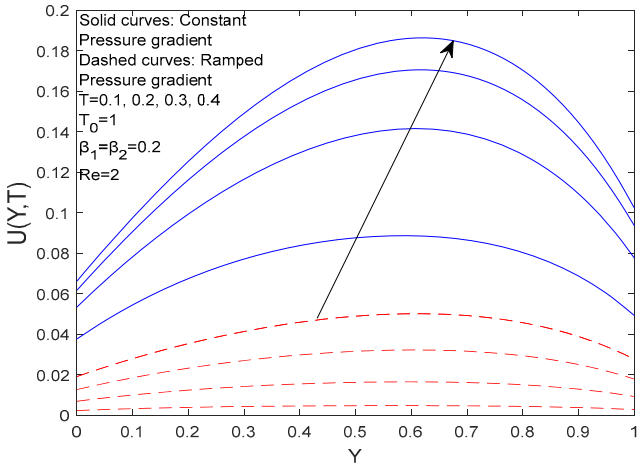


Fig.4. Velocity profile for different values of *T*, corresponding to constant and ramped pressure gradient.

Figures 1, 2 represent the velocity profile for distinct values of the slip parameter for the homogenous slip boundary condition. It is noticed that the velocity amplifies with an increase in the slip parameter $\beta$. The velocity is noted to be faster in the case of a constant pressure gradient and gradual in the case of a ramped pressure gradient. Figure 3 shows the velocity profile for different values of $(\mathrm{Re})$ for both constant and ramped pressure gradient where a rise in $(\mathrm{Re})$ indicates mass injection at the bottom wall for both situations. It is noticed that a rise in $(\mathrm{Re})$ results in a lower magnitude of the velocity in both cases, this happens due to the lower speed up rate of the fluid in the flow direction sourced by the pressure gradients for a high level of the Reynolds number. Based on this inference the velocity equation is non-dimensionalized by a velocity dependent on a pressure gradient. Figure 4 is the velocity profile for different values of $(T)$, the velocity was noticed to increase with time, the unsteady velocity is observed to decompose with time so that the steady state velocity is reached. The effect of the ramped pressure gradient is that the motion of the fluid in the channel is slower with ramped pressure gradient compared to the motion of the fluid with constant pressure gradient.

**CASE II**: Non homogenous slip boundary condition.

We present the velocity profiles of the flow of an incompressible viscous fluid assuming a ramped pressure gradient as well as non-homogenous slip coefficients represented by the situation when $\beta_1$ is different from $\beta_2$.

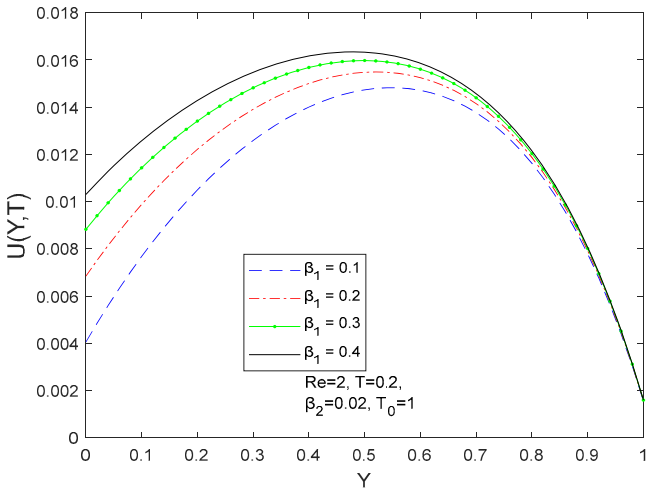


Fig.5. Velocity profile for different values of $\beta_1$, corresponding to ramped pressure gradient.

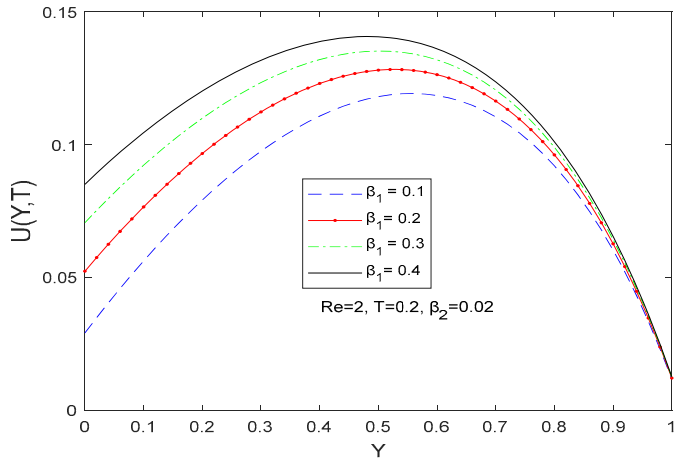


Fig.6. Velocity profile for different values of $\beta_1$, corresponding to constant pressure gradient.

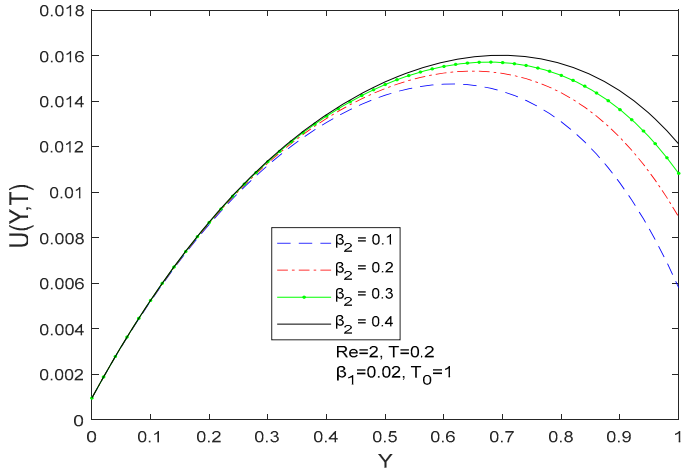


Fig.7. Velocity profile for different values of $\beta_2$, corresponding to ramped pressure gradient.

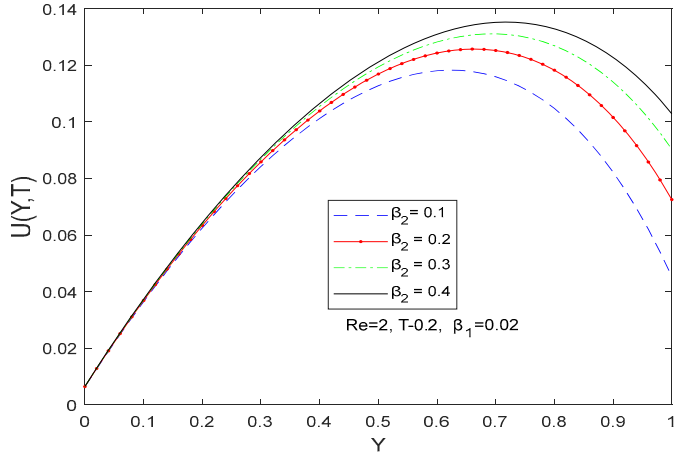


Fig.8. Velocity profile for different values of $\beta_2$, corresponding to constant pressure gradient.

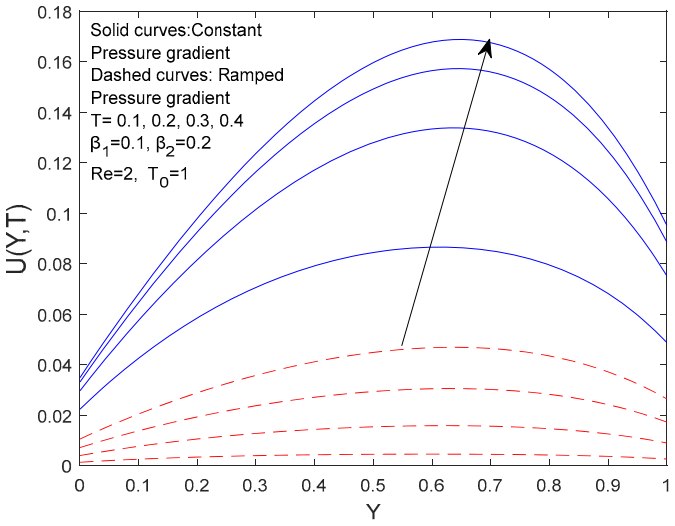


Fig.9. Velocity profile for different values of *T,* corresponding to constant and ramped pressure gradient.

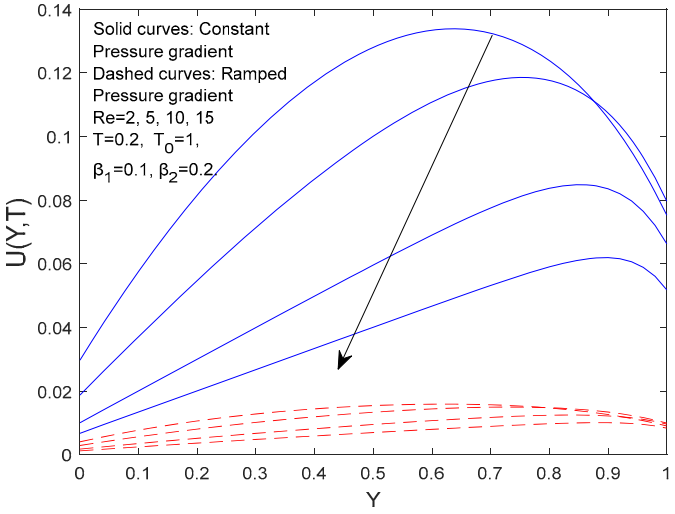


Fig.10. Velocity profile for different values of $\mathrm{Re}$ corresponding to constant and ramped pressure gradient.

Figures 5-8 are the velocity profiles for different values of the slip parameters $(\beta_1)$ and $(\beta_2)$, representing the non-homogenous slip boundary condition. It is noticed that a increase in the slip parameter amplifies n the flow velocity for both the constant and the ramped pressure gradient. The velocity in the case of a ramped pressure gradient is noticed to be slow compared to the constant pressure gradient. Figure 9 is the velocity profile for different values of time, it is observed that the magnitude of velocity rises with time, also an increase in time decomposes the transitory velocity and then the steady state velocity is reached. Figure 10 represents the velocity profile for different values of $(\mathrm{Re})$, for both the constant and ramped pressure gradient. it is noticed that a rise in $(\mathrm{Re})$ which indicates mass injection at the bottom plate, results in a lower magnitude of the velocity in both cases, this happens due to the lower speed up rate of the fluid in the flow direction by the pressure gradient for a high level of the Reynolds number. Based on this inference the velocity equation is non-dimensionalized by velocity dependent on the pressure gradient.

Table 1. Skin friction coefficient at $Y = 0$ , and $Y = 1$ for different values of $T$ and Re for homogenous and non-homogenous slip boundary conditions.

| Skin friction at $Y = 0$ | | | | Skin friction at $Y = 1$ | |
|---|---|---|---|---|---|
| $T$ | Re | Homogenous slip $T_0 = 0.1$, $\beta_1 = \beta_2 = 0.2$ | Non-homogenous slip $T_0 = 0.1$, $\beta_1 = 0.2$, $\beta_2 = 0.01$ | Homogenous slip $T_0 = 0.1$, $\beta_1 = \beta_2 = 0.2$ | Non-homogenous slip $T_0 = 0.1$, $\beta_1 = 0.2$, $\beta_2 = 0.01$ |
| *0.2* | *2.0* | *0.0345* | *0.0342* | *−0.0460* | *−0.0819* |
| | *4.0* | *0.0288* | *0.0287* | *−0.0500* | *−0.1011* |
| | *6.0* | *0.0239* | *0.0239* | *−0.0520* | *−0.1187* |
| | *8.0* | *0.0200* | *0.0200* | *−0.0521* | *−0.1333* |
| | *10.0* | *0.0170* | *0.0170* | *−0.0508* | *−0.1441* |
| *0.4* | *2.0* | *0.0958* | *0.0926* | *−0.1382* | *−0.2226* |
| | *4.0* | *0.0731* | *0.0722* | *−0.1453* | *−0.2724* |
| | *6.0* | *0.0564* | 0.0562 | *−0.1423* | *−0.3082* |
| | *8.0* | *0.0449* | *0.0449* | *−0.1338* | *−0.3306* |
| | *10.0* | *0.0370* | *0.0370* | *−0.1239* | *−0.3437* |
| Steady state | *2.0* | *0.3563* | *0.3256* | *−0.5616* | *−0.7889* |
| | *4.0* | *0.2357* | *0.2286* | *−0.5294* | *−0.9176* |
| | *6.0* | *0.1651* | *0.1639* | *−0.4696* | *−0.9744* |
| | *8.0* | *0.1248* | *0.1246* | *−0.4134* | *−0.9952* |
| | *10.0* | *0.1000* | *0.1000* | *−0.3667* | *−1.0001* |

Table 1 shows the skin frictions at the top and bottom plates for both homogenous and non-homogenous slip boundary conditions. It is noticed that the skin friction increases as the time increase for the bottom plate for both homogenous and non-homogenous slip boundary conditions. However, the skin friction has been observed to decrease as the time increases at the top plate for both homogenous and non-homogenous slip boundary condition. In addition, the skin friction has been noticed to decrease as $(\mathrm{Re})$ increases at the bottom plate. This is due to presence of mass injection, reducing the skin friction at the bottom plate for both homogenous and non-homogenous boundary conditions. While at the top plate the skin

friction is noticed to grow in the case of the homogenous slip boundary condition with growing $(\mathrm{Re})$ and the skin friction lessens with improving $(\mathrm{Re})$ for the non-homogenous slip boundary condition.

Table 2. Verifying the current result with the work of Fang [2] for the flow velocity.

| Velocity profile | | | |
|---|---|---|---|
| $T$ | $Y$ | Current result at $T_0 = 0.1, \mathrm{Re} = 5, \beta_1 = \beta_2 = 0$ | Fang (2004) |
| *0.2* | *0.2* | *0.0351* | *0.0367* |
| | *0.4* | *0.0646* | *0.0686* |
| | *0.6* | *0.0831* | *0.0897* |
| | *0.8* | *0.0761* | *0.0828* |
| | *10* | *0.0000* | *0.0000* |
| *0.4* | *0.2* | *0.0376* | *0.0376* |
| | *0.4* | *0.0711* | *0.0712* |
| | *0.6* | *0.0937* | *0.0939* |
| | *0.8* | *0.0868* | *0.0871* |
| | *10* | *0.0000* | *0.0000* |
| Steady state | *0.2* | *0.0377* | *0.0377* |
| | *0.4* | *0.0713* | *0.0713* |
| | *0.6* | *0.0941* | *0.0941* |
| | *0.8* | *0.0873* | *0.0873* |
| | *10* | *0.0000* | *0.0000* |

Table 3. Verifying the current result with the work of Fang [2] for the skin frictions.

| Skin friction at $Y = 1$ | | | | Skin friction at $Y = 0$ | | | |
|---|---|---|---|---|---|---|---|
| $T$ | Re | Current result at $T_0 = 0.1$, $\beta_1 = \beta_2 = 0$ | Fang (2004) | $T$ | Re | Current result at $T_0 = 0.1$, $\beta_1 = \beta_2 = 0$ | Fang (2004) |
| *0.2* | *2.0* | *−0.5292* | *−0.5859* | 0.2 | *2.0* | *0.2964* | *0.3175* |
| | *4.0* | *−0.6532* | *−0.7150* | | *4.0* | *0.2155* | *0.2241* |
| | *6.0* | *−0.7573* | *−0.8091* | | *6.0* | *0.1602* | *0.1629* |
| | *8.0* | *−0.8323* | *−0.8661* | | *8.0* | *0.1238* | *0.1245* |
| | *10.0* | *−0.8802* | *−0.8979* | | *10.0* | *0.0998* | *0.1000* |
| *0.3* | *2.0* | *−0.6135* | *−0.6327* | *0.3* | *2.0* | *0.3277* | *0.3347* |
| | *4.0* | *−0.7397* | *−0.7553* | | *4.0* | *0.2274* | *0.2295* |
| | *6.0* | *−0.8238* | *−0.8318* | | *6.0* | *0.1636* | *0.1640* |
| | *8.0* | *−0.8721* | *−0.8747* | | *8.0* | *0.1246* | *0.1247* |
| | *10.0* | *−0.8995* | *−0.9001* | | *10.0* | *0.1000* | *0.1000* |
| Steady state | *2.0* | *−0.6566* | *−0.6566* | Steady state | *2.0* | *0.3435* | *0.3435* |
| | *4.0* | *−0.7687* | *−0.7687* | | *4.0* | *0.2314* | *0.2314* |
| | *6.0* | *.−0.8359 .* | *−0.8359* | | *6.0* | *0.1642* | *0.1642* |
| | *8.0* | *−0.8754* | *−0.8754* | | *8.0* | *0.1247* | *0.1247* |
| | *10.0* | *−0.9001* | *−0.9001* | | *10.0* | *0.1000* | *0.1000* |

## 4. Conclusion

A study on the influence of velocity slip on the transitory flow formation of an incompressible fluid in a porous channel assuming a ramped pressure gradient along the flow direction has been conducted. The mathematical equation governing the flow was modelled and solved semi-analytically by the Laplace transformation technique. The numerical results were computed by MATLAB software to generate graphs and tables and the effects of the important parameters governing the flow were discussed. It was found that an increase in the slip parameter increases the flow velocity for both the ramped pressure gradient and constant pressure gradient.

### Appendix

$$Q_1 = \cosh(\delta) + \beta_2\left(\frac{\mathrm{Re}}{2}\right)\cosh(\delta) + \beta_2\delta\sinh(\delta),$$

$$Q_2 = \sinh(\delta) + \beta_2\left(\frac{\mathrm{Re}}{2}\right)\sinh(\delta) + \beta_2\delta\cosh(\delta), \qquad Q_3 = \frac{\bar{F}(s)}{s}exp\left(-\frac{\mathrm{Re}}{2}\right),$$

$$Q_4 = 1 - \beta_1\left(\frac{\mathrm{Re}}{2}\right), \qquad Q_5 = \beta_1\delta, \qquad Q_6 = \frac{\bar{F}(s)}{s},$$

$$C_1 = -\left[\frac{C_2Q_2}{Q_1}\right] - \frac{Q_3}{Q_1}, \qquad C_2 = -\left[\frac{Q_3Q_4 - Q_6Q_1}{Q_5Q_1 + Q_2Q_4}\right],$$

$$P_1 = 1 - \beta_1\mathrm{Re}, \qquad P_2 = exp(\mathrm{Re})(1 + \beta_2\mathrm{Re}), \qquad P_3 = P_1 - P_2, \qquad P_4 = \beta_1 + \beta_2,$$

$$D_1 = \frac{1}{\mathrm{Re}} + D_2\mathrm{Re}P_1 - \beta_1, \qquad D_2 = \frac{1 + P_4}{P_3\mathrm{Re}}$$

## Nomenclature

$u$ – dimensional velocity component along the $x$ axis $(m/s)$

$h$ – channel width $(m)$

$y$ – dimensional coordinate in $y-$ direction

$Y$ – dimensionless coordinate in $y-$ direction

$t$ – dimensional time $(s)$

$T$ – dimensionless time $(s)$

$s$ – Laplace parameter

$\bar{U}$ – dimensionless velocity in the Laplace domain $(m/s)$

$U$ – dimensionless velocity in time domain $(m/s)$

$U_0$ – dimensionless reference velocity $(m/s)$

$\frac{dp}{dx}$ – dimensional ramped pressure gradient $\left(N/m^2\right)$

$F(T)$ – dimensionless ramped pressure gradient $\left(N/m^2\right)$

Re – Reynolds number

$\mu$ – dynamic viscosity $\left(kgm^{-1}s^{-1}\right)$

$v$ – kinematic viscosity $\left(m^2 s^{-1}\right)$

$v_w$ – suction/injection velocity $\left(m/s\right)$

$\rho$ – density of the fluid $\left(kgm^{-3}\right)$

$\beta_1', \beta_2'$ – dimensional slip coefficients

$\beta_1, \beta_2, \beta$ – dimensionless slip coefficients

## References


[1] Liu Q. and Prosperitti A. (2011): *Pressure-driven flow in a channel with porous walls*.– Journal of Fluid Mechanics, vol.679, pp.77-100.

[2] Fang T. (2004): *Further discussion on the incompressible pressure-driven flow in a channel with porous walls*.– International Communication of Heat Mass Transfer, vol.31, No.4, pp.487-500.

[3] Fang T. (2004): *A note on the incompressible Couette flow with porous walls*.– International Communication of Heat Mass Transfer, vol.31, No.1, pp.31-41.

[4] Hafeez H.Y. and Ndikilar C.E. (2014): *Flow of viscous fluid between two parallel porous plates with bottom injection and top suction*.– Progress in Physics, vol.10, No.1, pp.49-51.

[5] Khaled A.-R.A. and Vafai K. (2004): *The effect of slip condition on Stokes and Couette flows due to an oscillating wall: exact solutions*.– International Journal of Non Linear Mechanics, vol.39, pp.795-809.

[6] Jha B.K. and Jibril H.M. (2013): *Unsteady hydromagnetic Couette flow due to ramped motion of one of the plates*.– International Journal of Applied Mechanics and Engineering, vol.18, No.4, pp.1039-1056.

[7] Jha B.K. and Gambo Y.Y. (2019): *Dufour effect with ramped wall temperature and specie concentration on natural convection flow through a channel*.– MDPI, vol.1, No.1, pp.111-130.

[8] Jha B.K. and Gambo D. (2021): *Hydrodynamic effect of slip boundaries and exponentially decaying/growing time-dependent pressure gradient on Dean flow*.– Journal of Egypt Mathematical Society, vol.29, No.11, p.15, DOI:10.1186/s42787-021-00120-z.

[9] Ahmad S., Chishtie F. and Mahmood A. (2017): *Analytical technique for MHD fluid flow of a periodically accelerated plate with slippage*.– European Journal of Mechanics, vol.65, pp.192-198, DOI:/10.1016/j.euromechflu.2017.03.012 S0997-7546(16)30337-5.

[10] Nagayama G., Matsumoto T. Fukushima, K. and Tsuruta T. (2017): *Scale effect of slip boundary condition at solid-liquid interface*.– Scientific reports, vol.7, Article No.43125, p.8.

[11] Wang C.Y. (2013): *The effect of slip on the flow in a rotating channel*.– Technical note, Chemical Engineering Communications, vol.200, pp.587-594.

[12] Fang T. and Lee C.F. (2006): *Exact solutions of incompressible Couette flow with porous walls for slightly rarefied gases*.– Heat Mass Transfer, vol.42, pp.255-262.

[13] Wang C.Y. (2012): *Brief review of exact solutions for slip-flow in ducts and channels*.– Journal of Fluid Engineering, vol.134, ID 094501-2.

[14] Jha B. K. and Danjuma Y.J. (2020): *Unsteady Dean flow formation in an annulus with partial slippage: A Riemann-Sum approximation approach*.– Results in Engineering, vol.5, Article No.100078, p.3.

[15] Jha B.K. and Aina B. (2016): *Role of suction/injection on steady fully developed mixed convection flow in a vertical parallel plate microchannel*.– Ain Shams Engineering Journal, vol.9, No.4, pp.2090-4479, doi.org/10.1016/j.asej.05.001.

[16] Ashwini B., Katagi N.N. and Rai A.S. (2017): *Analysis of laminar flow through a porous channel with velocity slip*.– Malaysian Journal of Mathematical Sciences, vol.11, No.3, pp.423-439.


Received: November 4, 2021
Revised: January 15, 2022